



ORIGINAL RESEARCH ARTICLE

Annealing Effect of High-Density Pulsed Electric Current Treatment on Cold-Rolled 6061 Aluminum Alloy

Yu Xiaoming, Gu Shaojie, Yoon Sungmin, Kimura Yasuhiro, Toku Yuhki, and Ju Yang

Submitted: 28 February 2023 / Revised: 4 July 2023 / Accepted: 12 July 2023 / Published online: 11 September 2023

The present study introduces a novel method of high-density pulsed electric current (HDPEC) as a substitute for the conventional annealing heat treatment process to relieve strain hardening in 6061 aluminum alloy (A6061) during the manufacturing process. The study investigates the effects of different HDPEC treatments on the strain-hardening relief of cold-rolled A6061, with a comparison to the traditional annealing heat treatment. The results reveal that the HDPEC-treated samples demonstrate a remarkable reduction of approximately 50% in strength and a considerable increase of approximately 200% in ductility, indicating complete strain-hardening relief of cold-rolled A6061. Consequently, the HDPEC treatment is faster and more efficient than the traditional annealing heat treatment. Furthermore, the HDPEC-treated samples display equivalent mechanical properties as the untreated ones after the final precipitation heat treatment, indicating that the HDPEC treatment has no detrimental effect on the materials. The microstructural characterization demonstrates that the HDPEC-induced microstructural modification through dislocation elimination and grain recovery leads to the strain-hardening relief of cold-rolled A6061. These findings suggest that the HDPEC treatment can even replace the hot-forming process of A6061, contributing to low-cost and high-efficient manufacturing.

Keywords 6061 aluminum alloy, dislocation, grain refinement, high-density pulsed electric current, strain hardening

1. Introduction

The 6061 aluminum alloy (A6061) is widely used in structural constructions, such as ships, aerocrafts, and automobiles, owing to its exceptional mechanical properties, corrosion resistance, and weldability. However, the excellent material properties make it challenging to be processed at room temperature. Typically, hot/warm forming is adopted to enhance the formability of aluminum alloys, which involves the recovery of microstructure during processing. However, these processes require preheating beforehand and maintaining a high temperature for hours, leading to significant energy consumption and greenhouse gas (GHG) emissions (Ref 1). Therefore, the need to suppress energy consumption and GHG emissions during the deformation process of A6061 is imperative. It is crucial to develop an environment-friendly manufacturing method to overcome the aforementioned problem. As such, the development of an innovative and sustainable method that can replace the hot/warm forming process while maintain-

ing or enhancing the material properties is of utmost significance (Ref 2). In addition, the T6 heat treatment is a widely employed process for enhancing the properties of A6061 aluminum alloy. It consists of a sequence of steps, starting with solution heat treatment and followed by artificial aging. During the aging stage, the controlled formation of Mg_2Si precipitates occurs, leading to the refinement of the microstructure and the enhancement of the alloy's hardness, yield strength, and resistance to deformation. This heat treatment process enables the alloy to attain a favorable combination of mechanical properties, rendering it highly suitable for a diverse range of demanding applications, including aircraft structures, automotive components, bicycle frames, sports equipment, and architectural structures.

Since the 1960 s, Troitskii and his co-workers have reported a stress drop phenomenon in metallic materials during tensile deformation when electric currents are applied (Ref 3). Since then, numerous studies have been conducted to investigate the effect of electric current on the mechanical properties of various materials. For instance, Xu et al. found that continuous application of electric current to the titanium alloy can accelerate the recrystallization rate and grain growth (Ref 4). Gu et al. reported that the strain hardening in Ni-based alloy IN718 and stainless steel SUS316 was rapidly removed by electric current treatment, and the mechanism was attributed to dislocation elimination and grain recovery (Ref 5, 6). Zheng et al. demonstrated that the solid solution treatment of A6061 was completed in 15 seconds by applying a high-density current (Ref 7). Perkins et al. also reported that the deformation resistance decreased when an electric current was applied to metals during plastic deformation (Ref 8). Related studies have also reported that this may be due to the combination of thermal (i.e., Joule heating) and athermal effects on rapid microstructural modification (Ref 5, 6, 9-17). Joule heating is the

Yu Xiaoming, Department of Micro-Nano Mechanical Science and Engineering, Graduate School of Engineering, Nagoya University, Nagoya 464-8603, Japan; and Daian Works, Kobe Steel Ltd., 1100 Daiiancho Umedo, Inabe, Mie 511-0284, Japan; and **Gu Shaojie**, **Yoon Sungmin**, **Kimura Yasuhiro**, **Toku Yuhki**, and **Ju Yang**, Department of Micro-Nano Mechanical Science and Engineering, Graduate School of Engineering, Nagoya University, Nagoya 464-8603, Japan. Contact e-mail: ju@mech.nagoya-u.ac.jp.

generation of heat when an electric current passes through a material due to resistance. In contrast, the athermal effect generally contains the electron wind force (EWF) (Ref 12, 13) resulting from the impact of electrons on atoms, as well as the phonon wind force (PWF) (Ref 14) or thermal compressive stress (Ref 15) caused by the thermal gradient around defects, which may play a more significant role in the microstructural modification of materials (Ref 16, 17). Despite many studies reporting the modification of metallic materials by electric current, the impact of electric current on cold-worked aluminum alloy A6061 and its potential as a replacement for traditional annealing heat treatment remains unclear (Ref 18). Therefore, this study aims to utilize a novel high-density pulsed electric current (HDPEC) method to substitute the annealing heat treatment for removing strain hardening caused by cold-rolling. Firstly, systematically investigate the effect of different HDPEC conditions on the recovery of mechanical properties of cold-rolled A6061, comparing the results to those obtained using traditional annealing heat treatment. Subsequently, microstructure characterization was performed to reveal the underlying mechanisms. The results demonstrate that the proposed method is a viable replacement for traditional annealing heat treatment in A6061 forming.

2. Material and Experimental Procedures

In this study, a cold-rolled A6061 sheet with a thickness reduction from 15 to 1 mm was used. The obtained sheet is a product of the manufacturing process and has not undergone T6 heat treatment yet. Table 1 shows the chemical composition of the as-received A6061. The geometric dimensions of the samples in this study were referenced to the ASTM A370 standard. Small-sized specimens were used with a width of 6.25 mm and a gauge length of 25 mm for the tensile part processed by wire-cutting, and the sample geometry is illustrated in Fig. 1. The tensile direction was along the cold rolling direction. The tensile test was conducted on a hydraulic-driven tensile testing machine (SHIMADZU) at room temperature with a loading speed of 1 mm/min. The application of HDPEC was performed on a fusing welding power supply (IS-300A, Amada) with the ability to set the time range at the millisecond level. In this study, a rectangular pulse current was employed, and its waveform is shown in Fig. 1.

The experimental plan of this study is listed in Table 2. Sample S0 was the as-received cold-rolled sample without HDPEC and annealing treatments. Samples S1-S5 were designed to verify the influence of increasing Joule heating (thermal effect) on the strain-hardening relief. Additionally, the current conditions for samples S1-S5 were determined based on the output capability of the power supply and the recrystallization temperature of the A6061, commonly in the range of 200-300 °C. Sample S6 was a fully annealed sample (410 °C for 90 min) for comparison. The preliminary research has demonstrated that sample S3 at the current density of 300 A/mm² for 200 ms, completely eliminated the strain hardening. Therefore, based on this current condition, we designed a series of thermal-equivalent experiments (S3-1 to S3-4, which have the same thermal effect) based on the formula $E \propto j^2 t$ $E \propto j^2 t$, where j is the current density and t is the duration. The purpose of the thermal-equivalent experiments was to investigate the influence of different athermal effects on the relief of strain

Table 1 Chemical composition of the as-received A6061 (wt.%)

Elements	Si	Fe	Cu	Mn	Mg	Cr	Ti	Al
wt.%	0.61	0.32	0.26	0.05	0.10	0.18	0.04	Bal.

hardening under identical thermal effects. Additionally, to examine the ultimate ability of the HDPEC treatment on strain-hardening relief, multiple HDPEC treatments were applied at each 12% strain for sample S7 and 8% strain for sample S8. The experiment processes for samples S7 and S8 were interrupted, meaning that after the tensile test, the samples were removed from the tensile machine, subjected to the HDPEC treatment, and then subjected to subsequent tensile tests in a cyclic manner until the fracture. Finally, samples S9 and S10 were designed to verify whether the HDPEC treatment affects the final T6 heat treatment (for the details, see Table 2). The T6 heat treatment contains the solution and aging treatment for the precipitation of the second phase. Furthermore, to ensure the reliability of the experimental results, all tensile tests were repeated at least twice.

The temperature rising of the HDPEC-treated samples was examined by non-contact infrared thermal sensors (GTL3ML-CF4 and GTL-2MH-FF). The measured temperature-time curves of each sample are shown in Fig. 2. For samples S1-S5, the temperatures are rapidly increased and then gradually cooled down with time, and the maximum temperature of the samples can be reached increases with the duration of the HDPEC, as shown in Fig. 2(a). Additionally, the thermal-equivalent experiments present almost the same maximum temperature at approximately 310 °C, but there are some differences in the heating rate, as shown in Fig. 2(b). For comparison, the Joule heating equation was also used to estimate the temperature rising during electric current treatment (Ref 19), $\Delta T = J^2 t \rho / (c_p d)$, where J is the current density, t duration time, ρ electrical resistivity, c_p specific heat capacity, d density of A6061. Hence, the maximum temperatures of the HDPEC-treated samples by measurement and numerical evaluation are listed in Table 2. The results show that the measured data and the numerical calculation results can be consistent, and the maximum temperature rising of all the HDPEC-treated samples was below 400 °C.

The surface morphology was observed using the scanning electron microscope (SEM, JSM-7200F, JEOL), and the elemental analysis was performed using the energy-dispersive x-ray spectroscopy (EDS) method attached to the SEM. In addition, changes in crystallographic properties after the HDPEC treatment were investigated using the x-ray diffraction (XRD) method. The experiment was carried out on a Rigaku x-ray analyzer using a copper target to generate x-rays with a scanning range from 30 to 90°. For the calculation of the dislocation density, the modified Williamson-Hall and Warren-Averbach methods (Ref 20-22) are adopted in this study. Moreover, the electron backscatter diffraction (EBSD) measurement was carried out to reveal the microstructure evolution, and the data processing was performed on the commercial software MATLAB with an open-source toolbox of MTEX.

The surface of the specimens was first polished using sandpaper (ranging from 500 to 4000 grit) to remove any

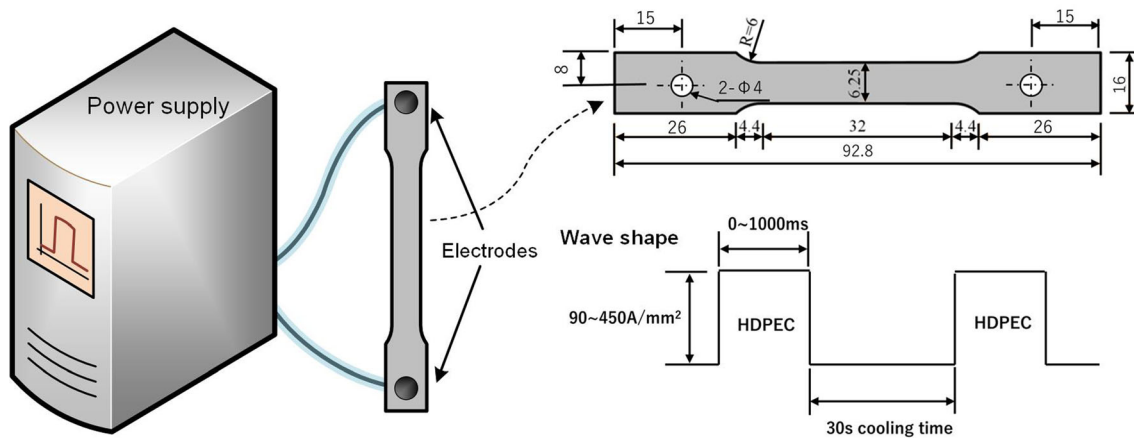


Fig. 1 Schematic diagram of the HDPEC application, including the geometry size of the tensile sample and the wave shape of the pulsed current

Table 2 The experimental plan of this study

Samples	HDPEC and/or heat treatment conditions	Maximum temperature, °C measured/numerical results
S0
S1	300 A/mm ² , 100 ms	114/152
S2	300 A/mm ² , 180 ms	250/273
S3	300 A/mm ² , 200 ms	310/303
S4	300 A/mm ² , 220 ms	324/333
S5	300 A/mm ² , 240 ms	370/364
S6	Annealing:410 °C, 90 min, furnace cooling	...
S3-1	120 A/mm ² , 1260 ms (Equivalent to S3)	303/303
S3-2	150 A/mm ² , 800 ms (Equivalent to S3)	308/303
S3-3	390 A/mm ² , 118 ms (Equivalent to S3)	313/303
S3-4	420 A/mm ² , 102 ms (Equivalent to S3)	304/303
S7	Applying 390 A/mm ² , 118 ms at each 12% strain	-/303
S8	Applying 390 A/mm ² , 118 ms at each 8% strain	-/303
S9	T6 heat treatment*	...
S10	390 A/mm ² , 118 ms + T6 heat treatment*	-/303

*T6 heat treatment: solution treatment at 555 °C for 2.5 hours followed by water quenching and aging treatment at 190 °C for 3.5 hours followed by furnace cooling.

roughness. Subsequently, polishing was performed using a 1- μ m diamond suspension to refine the surface further. Finally, an oxide polishing suspension with 0.04- μ m particles was used for the final polishing to effectively remove the plastic deformation layer on the material surface for better microstructural characterization.

3. Results

3.1 The Effect of HDPEC on Mechanical Properties of Cold-Rolled A6061

3.1.1 HDPEC Treatments at 300 A/mm² with Different Duration Times. Figure 3(a) shows the engineering stress-strain curves of the HDPEC-treated samples S1-S5, and the as-received cold-rolled sample S0 and annealing-treated sample S6 are also plotted for comparison. The commonly observed serrated tensile curves, characteristic of Al alloys, are also

evident in this study, especially for samples S3-S6. The serration phenomenon is related to the dislocation pinning and unpinning process with the solid solution atoms or precipitations, and the initial microstructural states are also affected (Ref 23, 24). The curves in the figure showed that the strain-hardening was gradually removed by HDPEC treatments, and the corresponding values of tensile strength and elongation are also shown in Fig. 3(b). Thereinto, sample S1 exhibited lower ductility compared to S0, which could be attributed to the lower current treatment intensifying dislocation entanglement. As a result, more severe stress concentration occurred during the subsequent tensile testing, leading to premature fracture. Additionally, the strain-hardening of sample S2 was partially relieved, while it was removed entirely once the HDPEC treatment exceeded a certain value, such as sample S3 at the current condition of 300 A/mm² for 200 ms. The tensile strength of sample S3 was dropped by approximately 50%, and the elongation increased by nearly 200% compared to the as-received sample S0. Although the strain hardening of

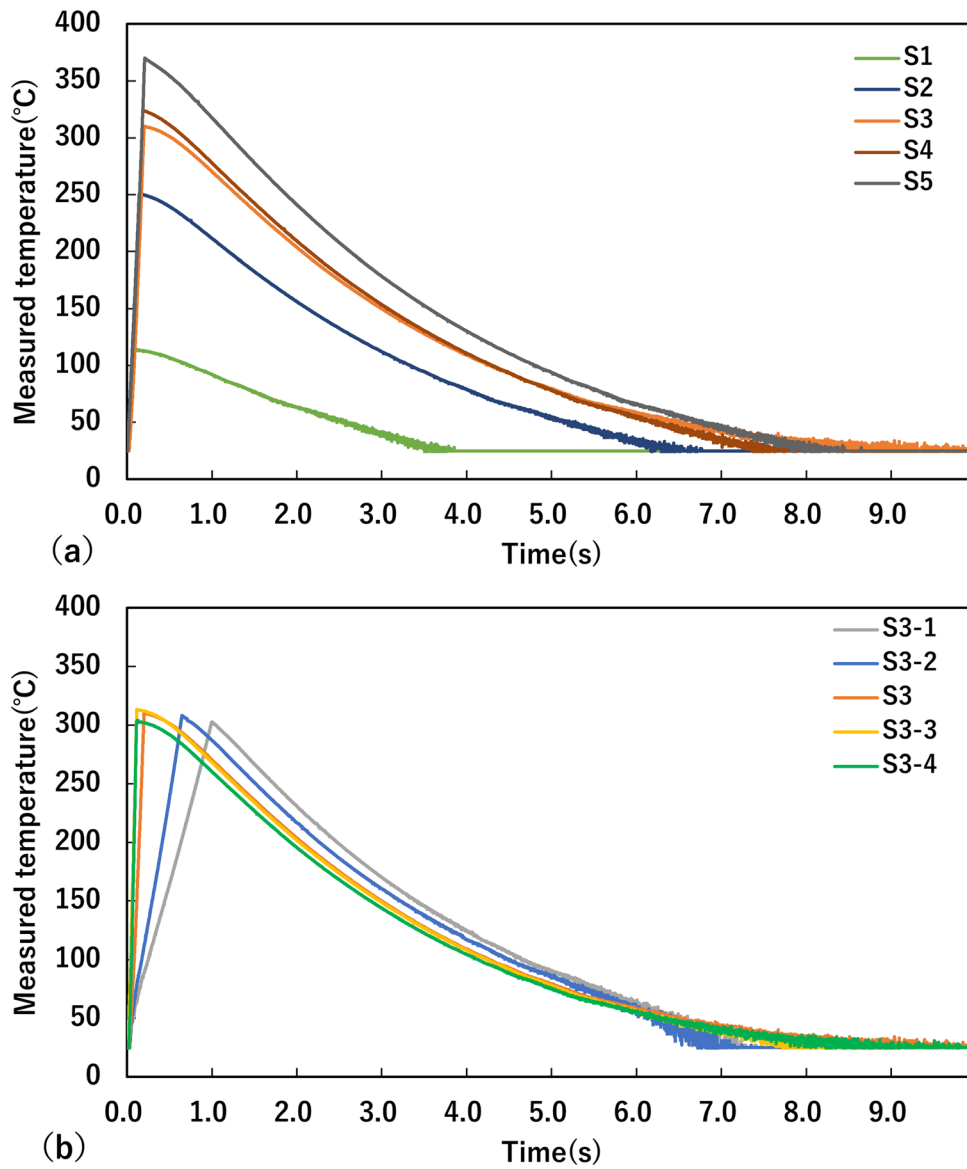


Fig. 2 Actual temperature measurement graphs of HDPEC-treated samples. (a) Samples S1-S5 with increased Joule heating and (b) thermal-equivalent samples

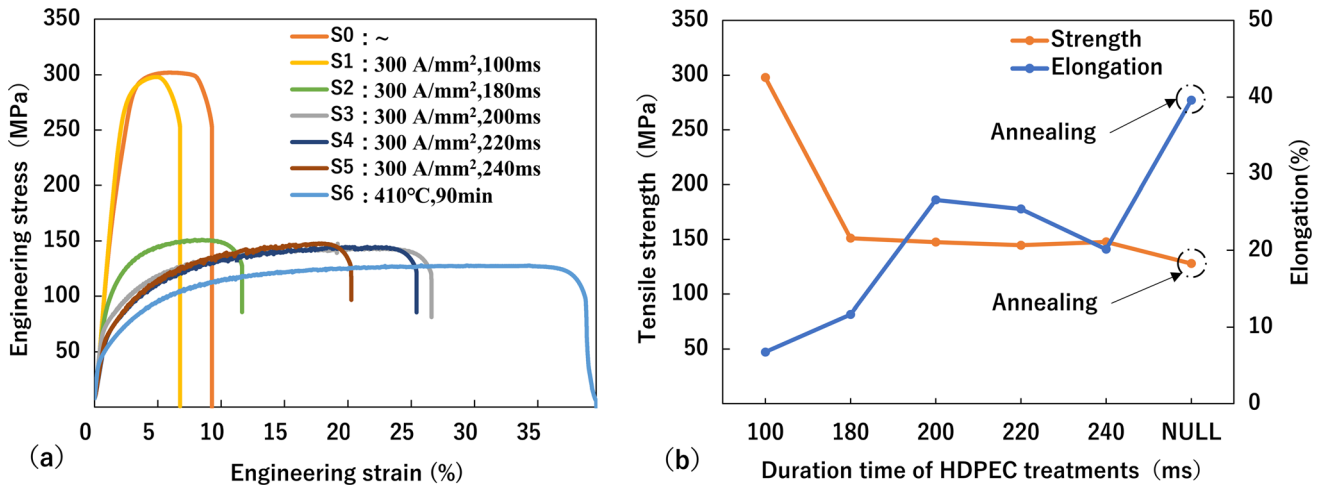


Fig. 3 (a) The engineering stress-strain curves and (b) bar diagram of mechanical properties of samples S0-S6

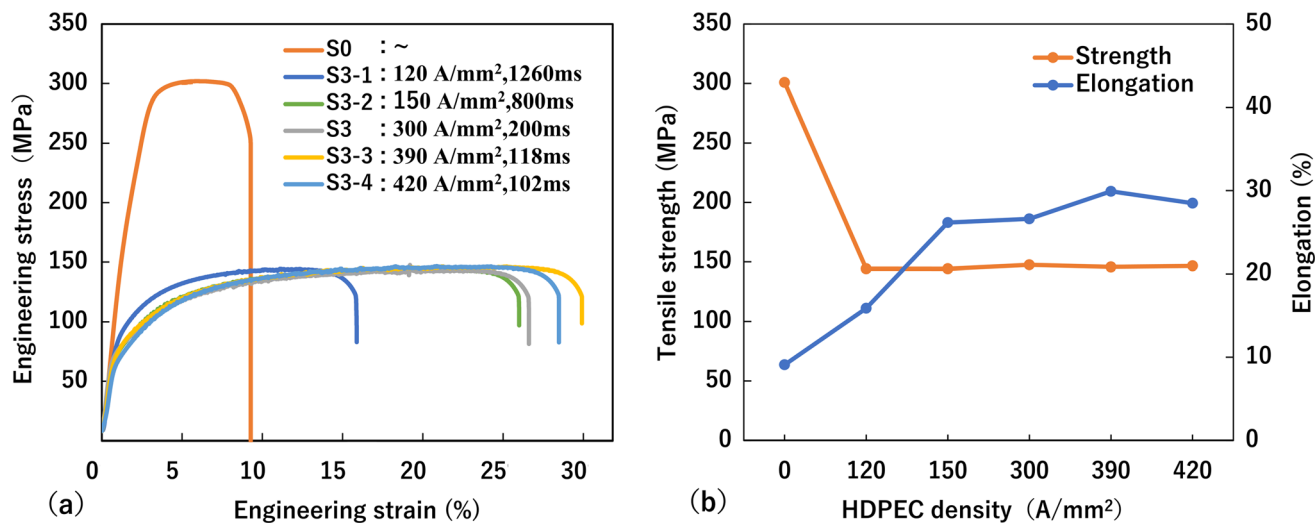


Fig. 4 (a) The engineering stress-strain curves and (b) bar diagram of mechanical properties of the thermal-equivalent samples

samples S4 and S5 was completely removed, their ductility was reduced, which could be attributed to the coarsening of their microstructure, thereby affecting the ductility. The conventional annealing heat treatment achieves the optimum strain-hardening removal with high ductility. Although the ductility of the HDPEC-treated experimental samples was inferior to that of the annealing treatment, they also succeeded in softening the material (reducing the strength) in a faster and more energy-efficient way, and they significantly improved processing efficiency.

3.1.2 Equivalent HDPEC-Treated Treatments. Figure 4 displays the stress-strain curves of the HDPEC-treated samples with equivalent treatments, resulting in complete strain-hardening relief and a notable strength reduction. However, sample S3-1 treated at a current density of 120 A/mm² exhibited weaker ductility than other equivalent HDPEC-treated cases. As the current density surpassed 120 A/mm², a significant improvement in ductility was observed, with optimum ductility achieved at 390 A/mm² (sample S3-3).

3.1.3 Multiple HDPEC-Treated Treatments. To examine the ultimate annealing effect of HDPEC application, multiple HDPEC treatments were applied at each 12% and 8% strains of samples S7 and S8, respectively, until fracture occurred. The resulting engineering stress-strain curves are illustrated in Fig. 5. Samples S7 and S8 were subjected to 3 and 6 HDPEC treatments, respectively, before fracturing. The maximum ductility reached 48% and 53%, respectively, which were higher than the annealing-treated sample S6 by an increasing rate of 13% and 18%, respectively. In addition, it is necessary to mention that sample S8 shows a higher ductility than sample S7, which may be due to the more frequent application of HDPEC allows for the timely removal of strain hardening within the sample, resulting in higher ductility.

3.1.4 Mechanical Properties After T6 Heat Treatment. Since T6 heat treatment is widely used in the process of A6061 aluminum alloy to realize higher strength and get well-balanced mechanical performance, the effect of HDPEC treatment on subsequent T6 heat treatment was investigated in this section. Figure 6 shows the stress-strain curves of both HDPEC-treated and untreated samples S9 and S10 after T6 heat treatment. Samples S9 and S10 exhibit almost identical

mechanical properties, with a tensile stress of 343 MPa and an elongation of 14%, indicating that the T6 heat treatment masked all previous processing history, including the HDPEC treatment. Therefore, HDPEC treatment can be an efficient and energy-saving manufacturing process for A6061 aluminum alloy. Moreover, it does not have any detrimental effect on the subsequent T6 heat treatment.

3.2 SEM Observation and EDS Analysis

Figure 7 illustrates the surface morphology and corresponding elemental distribution maps of samples S0, S3, and S6. For the as-received sample S0, the SEM images reveal the presence of white intermetallic compounds AlFeSi, identified by the elemental quantitative analysis of EDS. Some AlFeSi intermetallic compounds exhibit a fractured morphology, possibly due to cold rolling. However, after HDPEC treatment (sample S3) and annealing treatment (sample S6), there were no significant changes observed in the AlFeSi intermetallic compounds. Additionally, for samples S0, S3, and S6, the spatial distribution of alloying elements Mg and Si was found to be uneven, often segregating in certain regions.

The surface morphology and elemental distribution maps of samples S9 and S10 after T6 heat treatment are presented in Fig. 8. After T6 heat treatment, the AlFeSi intermetallic compounds did not undergo significant changes, but in some regions, gray Mg₂Si precipitation phases can be observed, as shown in Fig. 8(a) and (b). Furthermore, the spatial distribution of alloying elements Mg and Si became more uniform, which may facilitate the precipitation of the second phase Mg₂Si.

3.3 Crystallographic Changes Estimated by XRD Measurement

The XRD method was employed to investigate the influence of HDPEC treatment on the crystallography of cold-rolled 6061 aluminum alloy, as shown in Fig. 9. The XRD profiles of samples S0-S6 are presented in Fig. 9(a). Within the scanning range of 30-90°, diffraction peaks corresponding to the aluminum crystal phase of (111), (200), (220), (311), and (222) were observed. Additionally, peaks were observed at 40.5, 42.2, and 58.5°, which were identified as diffraction peaks of the intermetallic compound AlFeSi according to the SEM

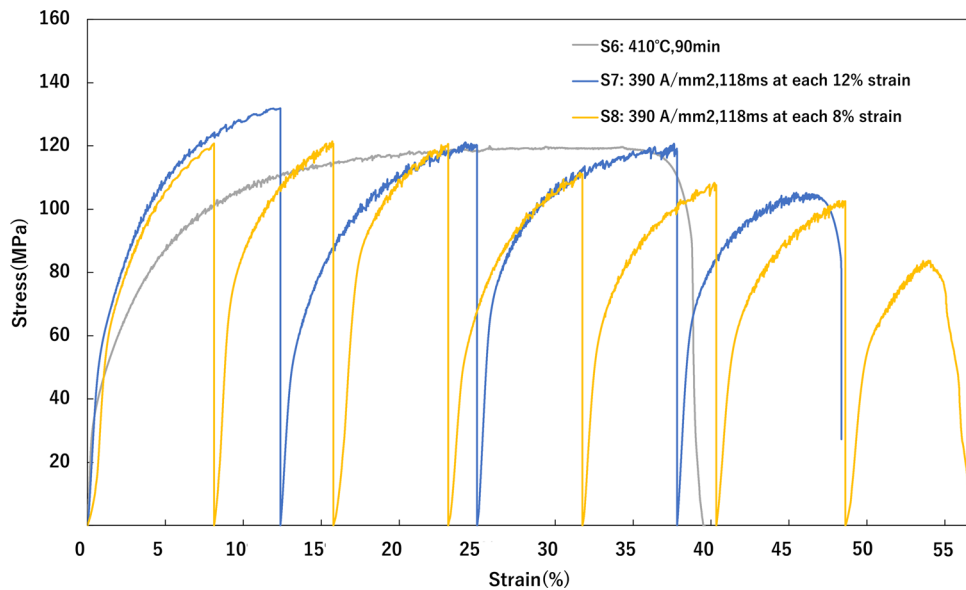


Fig. 5 The stress-strain curves of the multiple HDPEC-treated and annealed samples

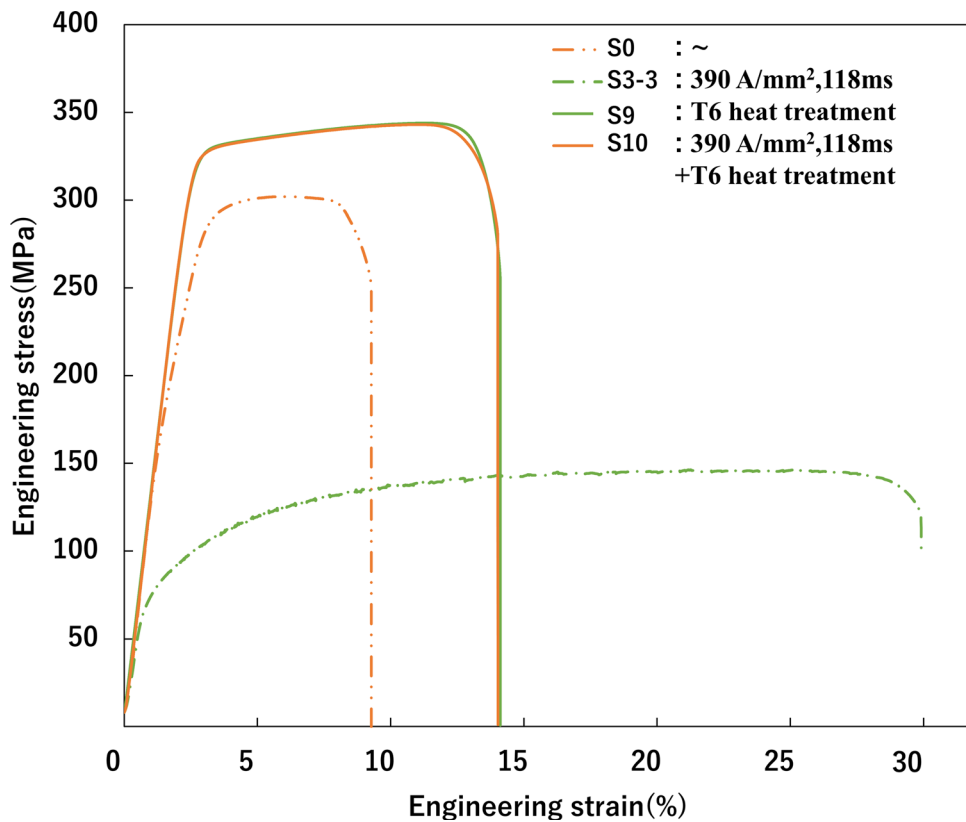


Fig. 6 The stress-strain curves after T6 heat treatment

observation and EDS analysis shown in Fig. 7. Furthermore, for the cold-rolled sample S0, the diffraction peaks of aluminum crystal phase exhibited lower intensity and larger full width at half maximum (FWHM), indicating the introduction of significant plastic deformation (or dislocations) within the crystal due to cold working. As the energy of the HDPEC treatment increased gradually (samples S1-S5), the diffraction peaks narrowed, and their intensities increased, indicating the removal

of dislocations within the crystal structure. The XRD profile of the annealed sample S6 also exhibited narrow and high diffraction peaks, indicating the removal of work hardening through the annealing process. Figure 9(b) illustrates the changes in the FWHM of the main diffraction peaks (111), (200), (220), and (311) of the aluminum crystal phase. As shown in the figure, HDPEC treatment significantly reduced the FWHM values of the aluminum diffraction peaks, and addi-

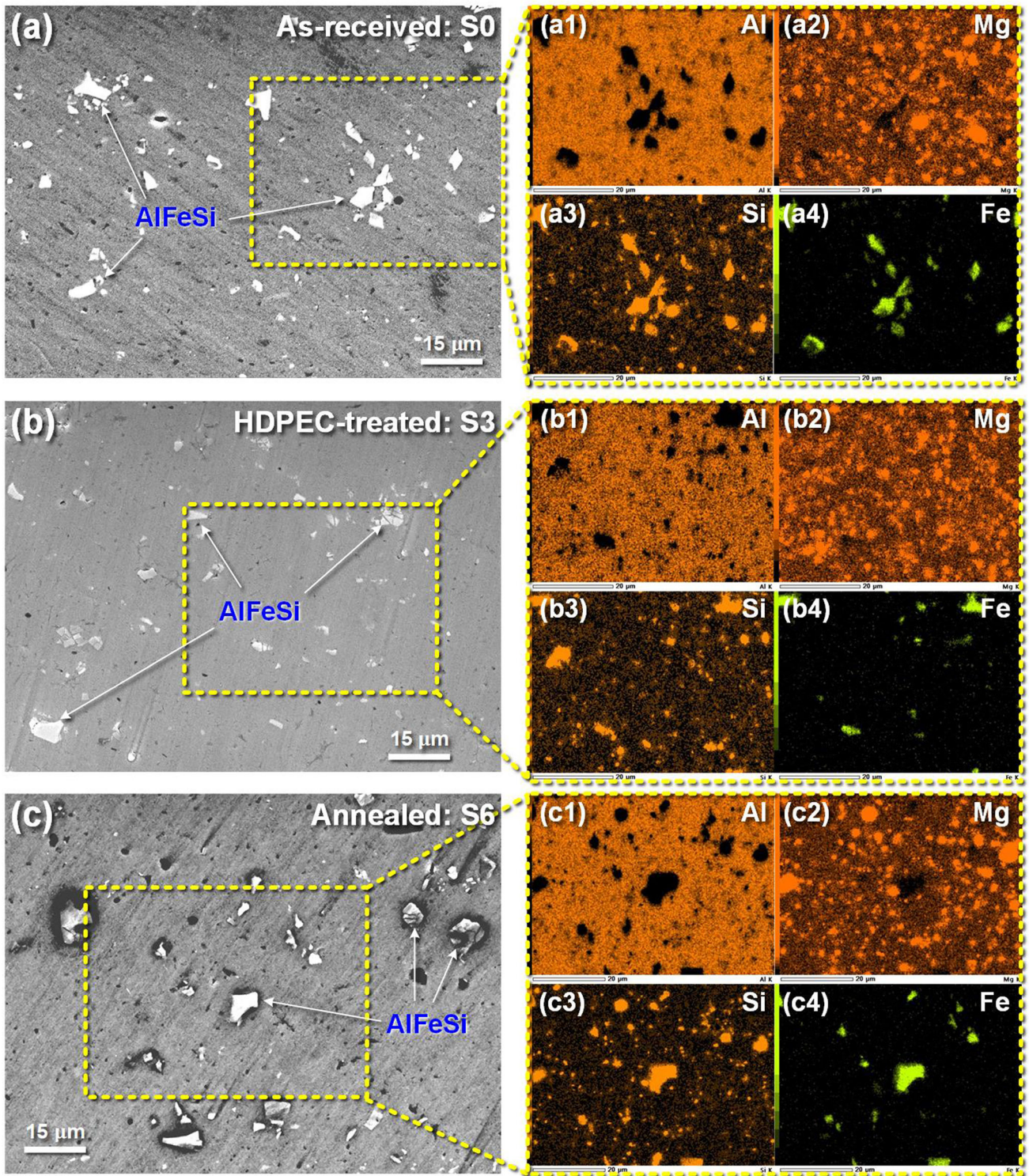


Fig. 7 SEM observation and EDS analysis of samples (a) S0, (b) S3 and (c) S6

tionally, the annealed sample S6 exhibited even lower FWHM values. The dislocation density of each sample was calculated using the XRD profile analysis method, as shown in Fig. 9(c). The cold-rolled sample S0 had a dislocation density of $1.03 \times 10^{15} \text{ m}^{-2}$, while after HDPEC treatment, the dislocation density of the material decreased to a level of $(0.1 \sim 0.2) \times 10^{15} \text{ m}^{-2}$. However, through annealing heat treatment, it decreased to $0.013 \times 10^{15} \text{ m}^{-2}$.

The XRD profiles of the A6061 after T6 heat treatment (samples S9 and S10) were also examined, as shown in Fig. 10. In addition to the diffraction peaks corresponding to the aluminum crystal phase and the intermetallic compound AlFeSi, we also observed diffraction peaks of Mg_2Si at 2θ angle of 40.5° , 48.6° , and 58.4° , which can be associated with the precipitation phase Mg_2Si observed in Fig. 8.

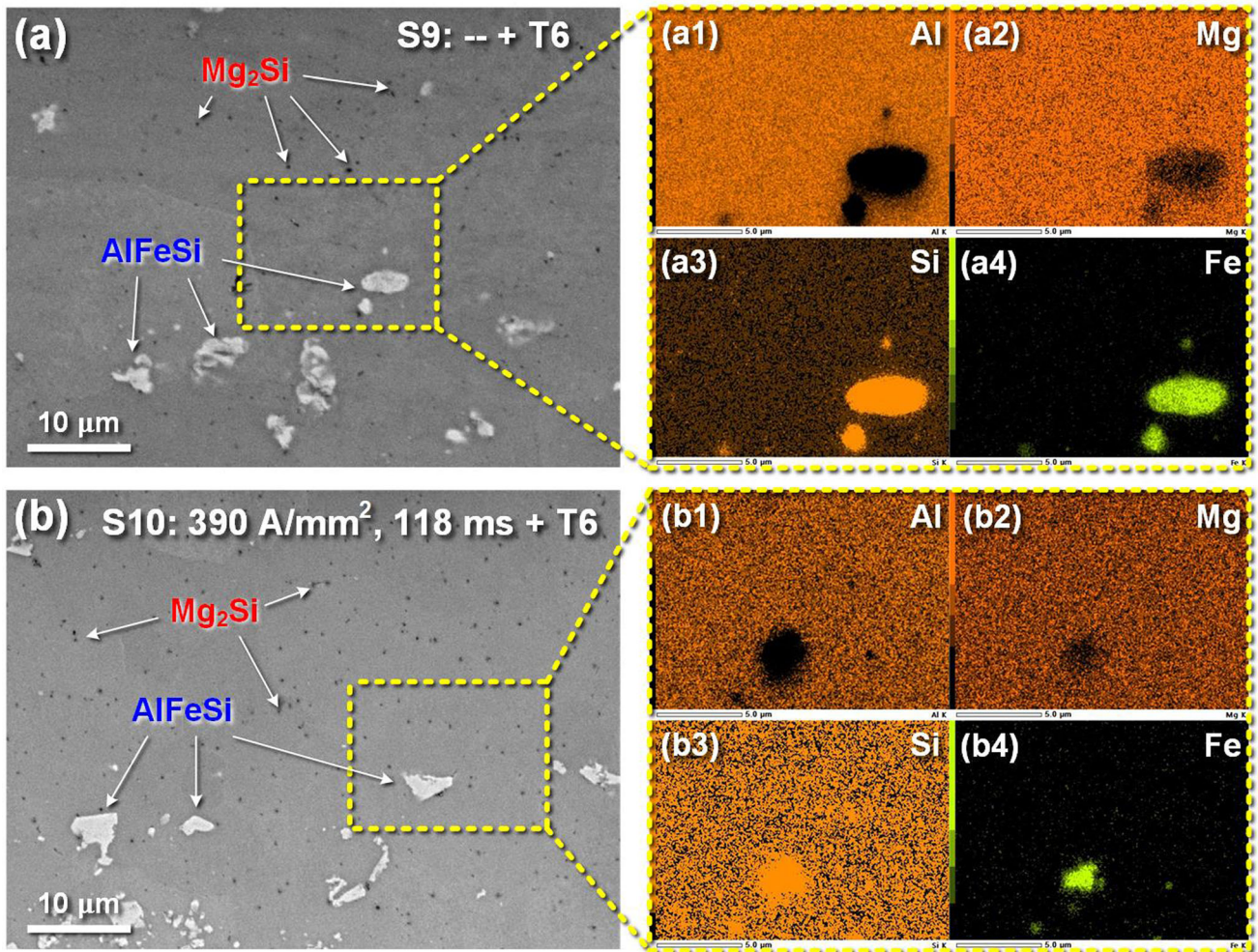


Fig. 8 SEM observation of samples (a) S9 and (b) S10 after T6 heat treatment

3.4 The Microstructure Evolution Using EBSD Measurement

In this study, EBSD measurement was employed to reveal the microstructural morphology evolution after HDPEC treatment, and the determined misorientation map, also known as kernel average misorientation (KAM), was used to evaluate the local deformation in grains. Figure 11(a), (b), and (c) shows the EBSD orientation maps of the as-received sample S0, HDPEC-treated sample S3-3, and annealed sample S6, with the mean grain sizes presented in Fig. 11(g). The as-received sample exhibited a typical cold-rolled grain morphology with an elongated grain shape along the rolling direction and a mean grain size of 19.6 μm . After HDPEC-treated at 390 A/mm² for 118 ms, the equiaxed and refined grain morphology was obtained with a mean grain size of 7.1 μm . The traditional annealing heat treatment can realize complete recrystallization but with a slight microstructure coarsening, where the grain growth resulted in a mean grain size of 23.2 μm .

Figure 11(d), (e), and (f) shows the KAM maps of the as-received sample S0, HDPEC-treated sample S3-3, and annealed sample S6, and the mean KAM values are also presented in Fig. 11(h). The KAM maps clearly show the local deformation within the crystalline grains and the evolution after different

treatments. The as-received sample showed a colored KAM map with many yellow colors (high KAM value), and the mean KAM value was approximately 0.6°. This value was significantly reduced to 0.198° after HDPEC treatment, implying the dislocation or local deformation was highly removed. For the traditional annealing heat treatment, the local deformation was totally alleviated.

Although the mechanical properties of the material were not affected by the HDPEC treatment after the subsequent T6 heat treatment, as shown in Fig. 6, it is still necessary to examine the microstructure of the material after the T6 heat treatment. The EBSD maps of the sample under T6 heat treatment and the sample first treated by HDPEC followed by T6 heat treatment are shown in Fig. 12. The microstructure in both conditions appears homogenized, but finer crystalline grains were obtained for the HDPEC-treated condition. However, the mechanical properties of both conditions were found to be identical. This can be attributed to the fact that a significant number of second phases precipitate after the T6 heat treatment, which is the main reason for the strengthening of A6061, while the strengthening of the material due to the finer grains is relatively weak.

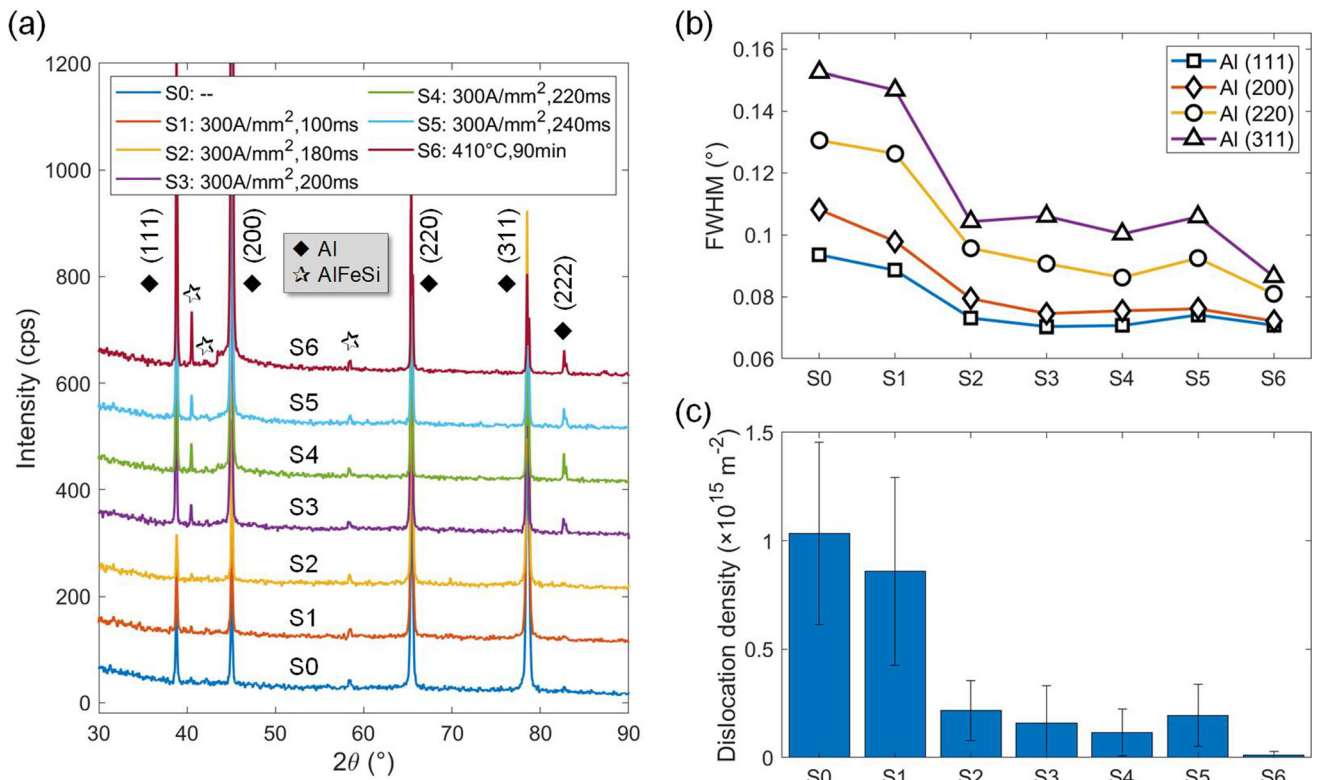


Fig. 9 Crystallographic analysis estimated by XRD measurement. (a) XRD profiles of samples S0-S6, (b) plots of the FWHM of the Al phase of each sample, and (c) dislocation density of each sample calculated by the XRD profile analysis method

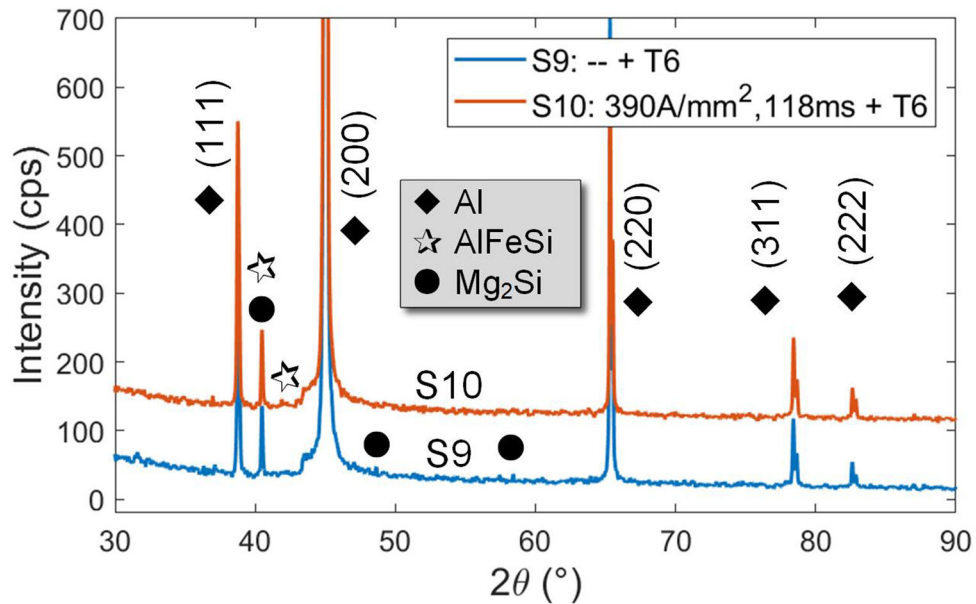


Fig. 10 XRD profiles of samples S9 and S10 after T6 heat treatment

4. Discussion

The HDPEC treatment has been demonstrated to effectively relieve the strain hardening of cold-rolled 6061 aluminum alloy. Specifically, the HDPEC condition of 300 A/mm² and 200 ms achieved a 50% reduction in strength and a 200% increase in

ductility, which is comparable to the annealed sample. Microstructural characterization revealed significant changes in local deformation (i.e., dislocation) and grain morphology following HDPEC treatment, with dislocations introduced by cold-rolling being almost completely eliminated and grain refinement achieved. Here, the reduction in strength of the

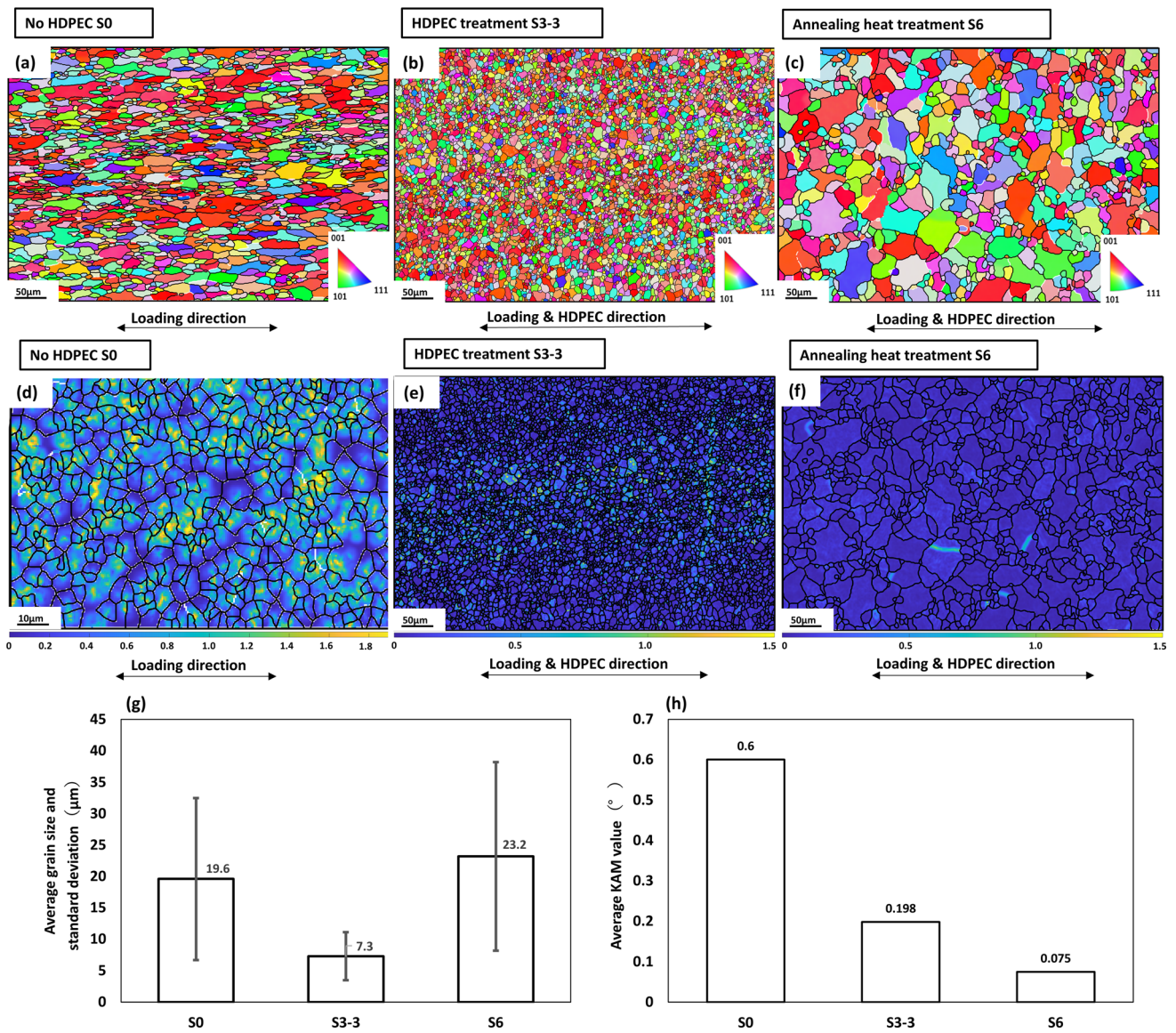


Fig. 11 The EBSD orientation maps of (a) as-received sample S0, (b) HDPEC-treated sample S3-3 and (c) annealed sample S6, the KAM maps of (d) as-received sample S0, (e) HDPEC-treated sample S3-3 and (f) annealed sample S6. (g) Mean grain size and (h) KAM values of each sample

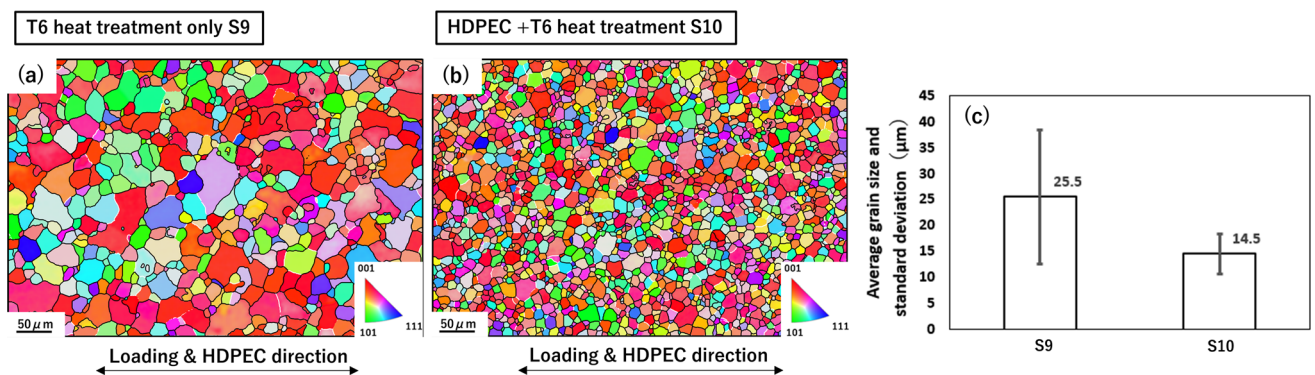


Fig. 12 The EBSD orientation maps of (a) HDPEC-untreated sample S9 and (b) HDPEC-treated sample S10 after T6 heat treatment, and (c) the mean grain size

material is mainly related to dislocation removal according to the strain-hardening law (Ref 25, 26). Although the refinement of the crystalline grains has the opposite effect—strengthening the material, the degree of the Hall-Petch effect (Ref 27, 28) is relative low. The recovery of the ductility was mainly related to dislocation elimination since the ductility is affected by the existing dislocations that hinder the multiplication and movement of new dislocations.

The HDPEC treatment demonstrated rapid microstructural modification in seconds at a low temperature of less than 310 °C, which is more efficient and effective compared to the traditional annealing treatment that requires a high temperature of 410 °C for 90 minutes. Related studies have also reported that this may be due to the combination of thermal and athermal effects on rapid microstructural modification, and the athermal effect, including EWF, PWF and thermal compressive stress, may play a more significant role (Ref 5, 6, 9-17). In this paper, the quantitative evaluation of the impact of EWF on dislocation motion was carried out. The evaluation of EWF on dislocation can be performed using the equation: $f_{EW} = (\rho_d/N_d)en_eJ/b$ $f_{EW} = (\rho_d/N_d)en_eJ/b$ (Ref 12, 29, 30). Parameter ρ_d/N_d ρ_d/N_d represents the specific dislocation resistivity of aluminum, which is approximately $1.8 \times 10^{-25} \Omega\cdot\text{m}^3$ at the temperature of 4.2 K (Ref 31). The value of e is the electron charge taken as 1.6×10^{-19} A·s, n_e is the electron density $1.8 \times 10^{29} \text{m}^{-3}$, and J denotes the J current density. b is the b Burgers vector with a length of 0.286 nm. Consequently, the EWF is estimated to be $f_{EW} = 5 \times 10^{-3}$ MPa for sample S3 treated at a current density of 300 A/mm². Furthermore, the Peierls-Nabarro (PN) stress (Ref 32, 33) presents the resistance stress required to move an individual dislocation. Experimental observations suggest that the PN stress for metals with a face-centered cubic lattice structure should range from $f_{PN} = 10^{-6} \sim 10^{-5} G(T)$ $G(T)$ (Ref 34, 35), where $G(T)$ $G(T)$ is the shear modulus of the material with respect to temperature. Considering the maximum temperature reached during the HDPEC treatment to be approximately 310 °C (sample S3), the shear modulus is estimated to be around 19 GPa (Ref 36). Consequently, the resistance stress for dislocation motion at elevated temperatures is approximately $f_{PN} = (19 \sim 190) \times 10^{-3}$ MPa. Thus, the EWF alone is insufficient to promote the movement of dislocations since the EWF is lower than the PN stress, $f_{EW} < f_{PN}$. Therefore, in this study, we believe that other athermal effect, such as PWF or thermal compressive stress induced by local heating (or thermal gradient) around the internal defect (e.g., dislocations) of the material during the electric current application, also contributes to the movement of dislocations and the final microstructural modification.

The relevant mechanisms in this study are described as follows. Firstly, the cold-rolled A6061 aluminum alloy contains a large number of dislocations, including movable dislocations and dislocation clusters (or cell structures). With the help of Joule heating, the athermal effect, such as EWF, PWF and thermal compressive stress, etc., promotes the rapid mobile dislocations until entangled with dislocation clusters or absorbed by grain boundaries. As a result, the HDPEC-treated samples induce more dislocation clusters and grain boundaries, which results in grain refinement at a lower temperature and shorter time. Additionally, the movement of dislocations induced by the athermal effect also results in a decrease of dislocation density, as shown in Fig. 9(c) and 11(h).

5. Conclusion

In this study, a novel high-density pulsed electric current (HDPEC) method was introduced to alleviate the strain hardening in A6061 aluminum alloy caused by cold-rolling. Some meaningful results are stated below.

1. The HDPEC-treated sample at the current condition of 300 A/mm² for 200 ms achieved approximately a 50% reduction in strength while a 200% increase in ductility, indicating complete strain-hardening relief, which is comparable with the annealed sample. The HDPEC treatment is more efficient and low-cost than traditional annealing heat treatment. Furthermore, multi-HDPEC treatment shows better deformation ability than annealed samples.
2. The HDPEC-treated sample shows similar mechanical properties with the untreated one after the final precipitation heat treatment, which suggests that the HDPEC treatment has no adverse effect on materials and can be used to alleviate the strain hardening in 6061 aluminum alloy during manufacturing.
3. The microstructure characterization revealed that the cold-rolled and elongated microstructure was recovered by fined and equiaxed grains with a low dislocation density after HDPEC treatment, implying the rapid modification of the microstructure was achieved. Moreover, the reason was attributed to thermal and athermal coupled effects.

The promising outcomes of this study suggest that HDPEC could serve as an alternative method to traditional annealing treatment for alleviating strain hardening in 6061 aluminum alloy during manufacturing. By enabling rapid and efficient microstructural modification, HDPEC could help to promote environmentally friendly manufacturing practices.

Acknowledgments

This work was supported by JSPS KAKENHI Grant-in-Aid for Challenging Research (Pioneering) 20K20531. The authors are also very grateful to Kobe Steel Ltd. and UACJ corporation for providing cold-rolled aluminum alloy sheets.

Conflict of interest

The authors declare that they have no conflict of interest.

References

1. O. Grydin, M. Stolbchenko, F. Nürnberger, and M. Schaper, Influence of Hot Deformation on Mechanical Properties and Microstructure of a Twin-Roll Cast Aluminium Alloy EN AW-6082, *J. Mater. Eng. Perform.*, 2014, **23**, p 937–943. <https://doi.org/10.1007/s11665-013-0816-4>
2. K. Zhao, R. Fan, and L. Wang, The Effect of Electric Current and Strain Rate on Serrated Flow of Sheet Aluminum Alloy 5754, *J. Mater. Eng. Perform.*, 2016, **25**, p 781–789. <https://doi.org/10.1007/s11665-016-1913-y>
3. O.A. Troitskii, Electromechanical Effect in Metals, *ZhETF Pisma Redaktsiiu.*, 1969, **10**, p 18–22
4. Z.S. Xu, Z.H. Lai, and Y.X. Chen, Effect of Electric Current on the Recrystallization Behavior of Cold Worked α -Ti, *Scr. Metall.*, 1988, **22**, p 187–190. [https://doi.org/10.1016/S0036-9748\(88\)80331-4](https://doi.org/10.1016/S0036-9748(88)80331-4)

5. S. Gu, Y. Cui, Y. Kimura, Y. Toku, and Y. Ju, Relief of Strain Hardening in Deformed Inconel 718 by High-Density Pulsed Electric Current, *J. Mater. Sci.*, 2021, **56**, p 16686–16696. <https://doi.org/10.1007/s10853-021-06344-9>
6. S. Gu, Y. Cui, S. Yoon, Z. Wang, Y. Kimura, Y. Toku, and Y. Ju, Rapid Anisotropy Recovery in Deformed FCC Metals by High-Density Pulsed Electric Current Treatment, *Vacuum*, 2022, **197**, p 110855. <https://doi.org/10.1016/j.vacuum.2021.110855>
7. Y.S. Zheng, G.Y. Tang, J. Kuang, and X.P. Zheng, Effect of Electropulse on Solid Solution Treatment of 6061 Aluminum Alloy, *J. Alloy. Compd.*, 2014, **615**, p 849–853. <https://doi.org/10.1016/j.jallcom.2014.07.062>
8. T.A. Perkins, T.J. Kronenberger, and J.T. Roth, Metallic Forging Using Electrical Flow as an Alternative to Warm/Hot Working, *J. Manuf. Sci. Eng.*, 2007, **129**, p 84–94. <https://doi.org/10.1115/1.2386164>
9. Y. Jiang, G. Tang, C. Shek, J. Xie, Z. Xu, and Z. Zhang, Mechanism of Electropulsing Induced Recrystallization in a Cold-Rolled Mg-9Al-1Zn Alloy, *J. Alloy. Compd.*, 2012, **536**, p 94–105. <https://doi.org/10.1016/j.jallcom.2012.05.014>
10. Y. Tang, A. Hosoi, Y. Morita, and Y. Ju, Restoration of Fatigue Damage in Stainless Steel by High-Density Electric Current, *Int. J. Fatigue*, 2013, **56**, p 69–74. <https://doi.org/10.1016/j.ijfatigue.2013.08.012>
11. W. Jin, J. Fan, H. Zhang, Y. Liu, H. Dong, and B. Xu, Microstructure, Mechanical Properties and Static Recrystallization Behavior of the Rolled ZK60 Magnesium Alloy Sheets Processed by Electropulsing Treatment, *J. Alloy. Compd.*, 2015, **646**, p 1–9. <https://doi.org/10.1016/j.jallcom.2015.04.196>
12. H. Conrad, Electroplasticity in Metals and Ceramics, *Mater. Sci. Eng. A*, 2000, **287**, p 276–287. [https://doi.org/10.1016/S0921-5093\(00\)00786-3](https://doi.org/10.1016/S0921-5093(00)00786-3)
13. C. Zhou, L. Zhan, C. Liu, and M. Huang, Insights into Electron Wind Force by a Helical Dislocation Reconfiguration, *IScience.*, 2023, **26**, p 106870. <https://doi.org/10.1016/j.isci.2023.106870>
14. C. Rudolf, R. Goswami, W. Kang, and J. Thomas, Effects of Electric Current on the Plastic Deformation Behavior of Pure Copper Iron, and Titanium, *Acta Mater.*, 2021, **209**, p 116776. <https://doi.org/10.1016/j.actamat.2021.116776>
15. S. Zhao, R. Zhang, Y. Chong, X. Li, A. Abu-Odeh, E. Rothchild, D.C. Chrzan, M. Asta, J.W. Morris, and A.M. Minor, Defect Reconfiguration in a Ti-Al Alloy via Electroplasticity, *Nat. Mater.*, 2020 <https://doi.org/10.1038/s41563-020-00817-z>
16. K. Jeong, S.W. Jin, S.G. Kang, J.W. Park, H.J. Jeong, S.T. Hong, S.H. Cho, M.J. Kim, and H.N. Han, Athermally Enhanced Recrystallization Kinetics of Ultra-Low Carbon Steel via Electric Current Treatment, *Acta Mater.*, 2022, **232**, p 117925. <https://doi.org/10.1016/j.actamat.2022.117925>
17. M.J. Kim, S. Yoon, S. Park, H.J. Jeong, J.W. Park, K. Kim, J. Jo, T. Heo, S.T. Hong, S.H. Cho, Y.K. Kwon, I.S. Choi, M. Kim, and H.N. Han, Elucidating the Origin of Electroplasticity in Metallic Materials, *Appl. Mater. Today.*, 2020, **21**, p 100874. <https://doi.org/10.1016/j.apmt.2020.100874>
18. S. Birinci, S. Basit, and N. Maraşlı, Influences of Directions and Magnitudes of Static Electrical Field on Microstructure and Mechanical Properties for Al-Si Eutectic Alloy, *J. Mater. Eng. Perform.*, 2022, **6**, p 5070–5079. <https://doi.org/10.1007/s11665-021-06564-9>
19. W. Zhang, M.L. Sui, Y.Z. Zhou, and D.X. Li, Evolution of Microstructures in Materials Induced by Electropulsing, *Micron*, 2003, **34**, p 189–198. [https://doi.org/10.1016/S0968-4328\(03\)00025-8](https://doi.org/10.1016/S0968-4328(03)00025-8)
20. T. Shintani and Y. Murata, Evaluation of the Dislocation Density and Dislocation Character in Cold Rolled Type 304 Steel Determined by Profile Analysis of x-ray Diffraction, *Acta Mater.*, 2011, **59**, p 4314–4322. <https://doi.org/10.1016/j.actamat.2011.03.055>
21. T. Ungár, I. Dragomir, Á. Révész, and A. Borbély, The Contrast Factors of Dislocations in Cubic Crystals: the Dislocation Model of Strain Anisotropy in Practice, *J. Appl. Crystallogr.*, 1999, **32**, p 992–1002. <https://doi.org/10.1107/S0021889899009334>
22. M. Jamal, S.J. Asadabadi, I. Ahmad, and H.R. Aliabad, Elastic Constants of Cubic Crystals, *Comput. Mater. Sci.*, 2014, **95**(592), p 9. <https://doi.org/10.1016/j.commatsci.2014.08.027>
23. Y. Zhang, J.P. Liu, S.Y. Chen, X. Xie, P.K. Liaw, K.A. Dahmen, J.W. Qiao, and Y.L. Wang, Serration and Noise Behaviors in Materials, *Prog. Mater. Sci.*, 2017, **90**, p 358–460. <https://doi.org/10.1016/j.pmatsci.2017.06.004>
24. Z. Sajuri, N.F. Mohamad Selamat, A.H. Baghdadi, A. Rajabi, M.Z. Omar, A.H. Kokabi, and J. Syarif, Cold-Rolling Strain Hardening Effect on the Microstructure, Serration-Flow Behaviour and Dislocation Density of Friction Stir Welded AA5083, *Metals.*, 2020, **10**, p 70. <https://doi.org/10.3390/met10010070>
25. G.I. Taylor, The mechanism of plastic deformation of crystals Part I Theoretical, *Proc. R. Soc. Lond. Ser. A Contain. Pap. Math. Phys. Character.*, 1934, **145**(855), p 362–387
26. P. Rodriguez, Sixty Years of Dislocations, *Bull. Mater. Sci.*, 1996, **19**, p 857–872. <https://doi.org/10.1007/BF02744623>
27. E.O. Hall, The deformation and ageing of mild steel: III discussion of results, *Proc. Phys. Soc. Sect. B.*, 1951, **64**(9), p 747. <https://doi.org/10.1088/0370-1301/64/9/303>
28. N.J. Petch, The Cleavage Strength of Polycrystals, *J. Iron Steel Inst.*, 1953, **174**, p 25
29. H. Conrad, A.F. Sprecher, The Electroplastic Effect in Metals, in: *Dislocations in Solids*, Elsevier, 497–541 (1989)
30. F.R.N. Nabarro, *Theory of Crystal Dislocations*, Clarendon Press, Oxford, 1967
31. R.A. Brown, Electrical resistivity of dislocations in metals, *J. Phys. F Met. Phys.*, 1977, **7**, p 1283–1295. <https://doi.org/10.1088/0305-4608/7/7/026>
32. R. Peierls, The Size of a Dislocation, *Proc. Phys. Soc.*, 1940, **52**, p 34. <https://doi.org/10.1088/0959-5309/52/1/305>
33. F.R.N. Nabarro, Dislocations in a Simple Cubic Lattice, *Proc. Phys. Soc.*, 1947, **59**, p 256. <https://doi.org/10.1088/0959-5309/59/2/309>
34. T. Suzuki and S. Takeuchi, Correlation of Peierls-Nabarro Stress with Crystal Structure, *Rev. Phys. Appl. Paris*, 1988, **23**, p 685–685. <https://doi.org/10.1051/rphysap:01988002304068500>
35. Y. Kamimura, K. Edagawa, and S. Takeuchi, Experimental Evaluation of the Peierls Stresses in a Variety of Crystals and their Relation to the Crystal Structure, *Acta Mater.*, 2013, **61**, p 294–309. <https://doi.org/10.1016/j.actamat.2012.09.059>
36. M. Janovská, H. Seiner, J. CIŽEK, P. Sedlák, and M. LAND, Evolution of Elastic Properties of Cold Sprayed Metal Coatings at Elevated Temperatures, *Acta Phys. Pol. A.*, 2018, **134**, p 794–798. <https://doi.org/10.12693/APhysPolA.134.794>

Publisher's Note Springer Nature remains neutral with regard to jurisdictional claims in published maps and institutional affiliations.

Springer Nature or its licensor (e.g. a society or other partner) holds exclusive rights to this article under a publishing agreement with the author(s) or other rightsholder(s); author self-archiving of the accepted manuscript version of this article is solely governed by the terms of such publishing agreement and applicable law.